Empirical Bayes Estimation of Tissue Scatterer Distribution from Ultrasonic Echo

Atsumi Ubukata Jing Zhu Yhisin Ho Norio Tagawa
Graduate School of System Design, Tokyo Metropolitan University
Hino, Tokyo, 191-0065, Japan
Email: tagawa@tmu.ac.jp

***Abstract*—In ultrasonic medical imaging, in addition to the boundaries of organs, blood vessels, etc., speckle patterns generated as interference of echoes from small scatterers in living tissue are often observed. Speckle pattern has information on the tissue properties and can be efficiently used as local position information for measuring tissue motions, for example. On the other hand, these are the main factor for lowering the image resolution. In this study, we aim to improve the resolution of ultrasonic imaging by restoring the scatterer distribution within the tissues from the echo. Statistics calculated from the restored scatterer distribution are expected to contribute to the construction of new indicators for tissue properties diagnosis.**

I. Introduction

In ultrasound medical imaging it is important that the boundaries and edges of organs, blood vessels and tumors are detected[1]-[3]. On the other hand, the reflection and distribution of small scatterers in living tissue has important information for diagnosing tissue properties. If the bandwidth of the transmitted pulse is sufficiently wide, that is, if very sharp pulses can be transmitted, high resolution imaging can be carried out and thus, the distribution of the scatterer producing the echoes can be measured exactly. However, in actual imaging, typical ultrasonic transducers have narrow band characteristics, and furthermore, in order to clearly obtain echoes, the transmitted pulse contains several cycles of sin waves. As a result, the reflectance distribution is convoluted with the transmitted signal, and the echo whose resolution is greatly reduced is reflected toward the transducer. These echo signals interfere with each other to generate speckle patterns, which make measurement of scatterer distribution difficult.

The speckle patterns are often used efficiently for medical diagnosis based on physician experience. These are also effective for tissue motion analysis using image processing. On the other hand, since the speckle patterns hinder the detection of small tumors, various suppression methods have been proposed[4]-[7]. Recently, studies to reduce speckle observation by actively imaging a small number of strong echo sources attract attention, which are based on compressed sensing and/or sparse modeling techniques [8]-[12]. In this strategy, only the echo intensity is taken into account and the speckle characteristics are ignored. Contrary to these facts, in this study, we aim to estimate the reflection distribution of scatterers, which is the source of the speckle pattern, from echo. If small scatterers can be accurately restored from the echoes, by subtracting the corresponding echoes from the entire echo, the images consisting only of sparse scatterers with strong reflection, i.e., contours of organs, blood vessels, tumors can be obtained by, for example, our super-resolution imaging method[13]. Namely, by separately processing small scatterers and large reflectors, both can be separately imaged, which leads to high resolution imaging.

This scatterers restoration must be treated as an ill-posed problem, because echoes occur via convolution process. It is not possible to uniquely restore the distribution of the scatterer from only the observed information, and observation noise is also likely to influence the solution. In order to solve these problems, it is necessary to (i) increase observation information and (ii) apply appropriate assumptions and constraints to the solution. The former can be realized, for example, by using harmonic echoes in addition to fundamental echoes. For measurement of harmonic echoes, we proposed techniques to improve SNR[14] and compensate for distortion caused by frequency dependent attenuation[15]. In this study, focusing on the latter, we consider the reflection distribution of small scatterers as a stochastic sequence arranged in the range direction, and we model it with autoregressive (AR) process usually used in random signal processing. The parameters of the AR model show correlations inherent in the reflection distribution, which are expected to parametrize the tissue properties. The ill-posed characteristics in this restoration problem are very strong, for example compared to blurred image restoration, because the frequency band not observed is so wide. Therefore, it is necessary to investigate the estimation possibility and accuracy of both the AR parameters and the reflection distribution itself. To realize that, we can apply the algorithm constructed in the time domain based on empirical Bayesian method[16][17]. As a first step of our future efforts, in this study we evaluate the performance through numerical simulation using data correctly fitted to the assumed model.

II. Method

A. Problem Formulation

Since the echo depends not only on the reflection of the scatterer but also on the transmittance and the diffraction, it is difficult to formulate the echo generation process considering all these properties. In this study, we define the equivalent reflectance that generates echo by convolution with the transmitted pulse.

978-1-5386-1023-7/17/$31.00

An N-dimensional vector $\boldsymbol{y}$ is defined as an observed RF echo signal, in which N corresponds to the number of time-sampling. We assume that $\boldsymbol{y}$ contains an additive white normal random numbers $\boldsymbol{n}$ with zero mean and variance σ_n^2 as observation noise. By using the N-dimensional vector $\boldsymbol{h}$ as the above mentioned equivalent reflectance, $\boldsymbol{y}$ can be formulated as follows:

$$\boldsymbol{y} = \boldsymbol{W}\boldsymbol{h} + \boldsymbol{n}, \tag{1}$$

where $\boldsymbol{W}$ is an $N \times N$ matrix representing convolution with the transmission pulse. As the width of the transmission pulse increases, the rank of $\boldsymbol{W}$ approaches zero. Therefore, we can simply restore $\boldsymbol{h}$ using $\boldsymbol{W}^+$ which is a pseudo-inverse of $\boldsymbol{W}$.

$$\hat{\boldsymbol{h}} = \boldsymbol{W}^+\boldsymbol{y}. \tag{2}$$

However, the solution is sensitive to the noise contained in $\boldsymbol{y}$, and furthermore, the information contained in $\boldsymbol{h}$ discarded by $\boldsymbol{W}$ can not be restored. Instead, by applying the AR model to $\boldsymbol{h}$ we consider the method to recover such discarded information by extrapolation.

The AR model is a general stochastic representation of random time series with correlation between components. Using i to indicate the order of the components, $\boldsymbol{h}$ is defined using the white normal noise ϵ_i with variance σ_h^2, as follows:

$$h_i = \sum_{j=1}^{P} a_j h_{i-j} + \epsilon_i, \tag{3}$$

Here, $\boldsymbol{a} \equiv \{a_1, a_2, ..., a_P\}$ is called the AR coefficient, and P is the order of the AR model and indicates the number of past components explicitly affecting the current component. The matrix and vector representation of Eq. 3 is as follows:

$$\boldsymbol{A}\boldsymbol{h} = \boldsymbol{\epsilon}. \tag{4}$$

For example, when $P = 2$, the matrix $\boldsymbol{A}$ is written as

$$\boldsymbol{A} = \begin{pmatrix} 1 & 0 & 0 & 0 & \cdots \\ -a_1 & 1 & 0 & 0 & \cdots \\ -a_2 & -a_1 & 1 & 0 & \cdots \\ 0 & -a_2 & -a_1 & 1 & \cdots \\ \vdots & \vdots & \vdots & \vdots & \ddots \end{pmatrix}. \tag{5}$$

From Eq. 4, $\boldsymbol{h}$ is a sample from the following multidimensional normal distribution.

$$p(\boldsymbol{h}|\boldsymbol{a}, \sigma_h^2) = \frac{1}{\sqrt{(2\pi\sigma_h^2)^N \det(\boldsymbol{A}^\top\boldsymbol{A})^{-1}}} \exp\left(-\frac{\boldsymbol{h}^\top\boldsymbol{A}^\top\boldsymbol{A}\boldsymbol{h}}{2\sigma_h^2}\right). \tag{6}$$

We can know that the mean of $\boldsymbol{h}$ is $\boldsymbol{0}$ and the variance-covariance matrix is $\boldsymbol{V}_h = \sigma_h^2(\boldsymbol{A}^\top\boldsymbol{A})^{-1}$.

B. Estimation Method based on Empirical Bayes

Considering that $\boldsymbol{y}$ contains observation noise, we aim to recover $\boldsymbol{h}$ in the time domain. From Eq. 1, the probabilistic density of $\boldsymbol{y}$ under the condition that $\boldsymbol{h}$ is given forms the following normal distribution.

$$p(\boldsymbol{y}|\boldsymbol{h}, \sigma_n^2) = \frac{1}{\sqrt{(2\pi\sigma_n^2)^N}} \exp\left[-\frac{(\boldsymbol{y}-\boldsymbol{W}\boldsymbol{h})^\top(\boldsymbol{y}-\boldsymbol{W}\boldsymbol{h})}{2\sigma_n^2}\right]. \tag{7}$$

The joint probability of $\boldsymbol{y}$ and $\boldsymbol{h}$ is derived using Eqs. 6 and 7 as follows:

$$p(\boldsymbol{y}, \boldsymbol{h}|\boldsymbol{a}, \sigma_n^2, \sigma_h^2) = \frac{\exp\left[-\frac{(\boldsymbol{y}-\boldsymbol{W}\boldsymbol{h})^\top(\boldsymbol{y}-\boldsymbol{W}\boldsymbol{h})}{2\sigma_n^2} - \frac{\boldsymbol{h}^\top\boldsymbol{A}^\top\boldsymbol{A}\boldsymbol{h}}{2\sigma_h^2}\right]}{(2\pi)^N\sqrt{{\sigma_n^2}^N{\sigma_h^2}^N\det(\boldsymbol{A}^\top\boldsymbol{A})^{-1}}}. \tag{8}$$

In general, $\{\sigma_n^2, \sigma_h^2, \boldsymbol{a}\}$ is estimated as the maximum likelihood estimator (MLE) using the probabilistic density of $\boldsymbol{y}$ obtained by marginalizing Eq. 8 with respect to $\boldsymbol{h}$.

$$\begin{aligned} p(\boldsymbol{y}|\boldsymbol{a}, \sigma_n^2, \sigma_h^2) &= \int p(\boldsymbol{y}, \boldsymbol{h}|\boldsymbol{a}, \sigma_n^2, \sigma_h^2) d\boldsymbol{h} \\ &= \frac{1}{\sqrt{(2\pi)^N \det\boldsymbol{\Lambda}}} \exp\left(-\frac{\boldsymbol{y}^\top\boldsymbol{\Lambda}^{-1}\boldsymbol{y}}{2}\right), \end{aligned} \tag{9}$$

$$\boldsymbol{\Lambda} = \sigma_h^2\boldsymbol{W}(\boldsymbol{A}^\top\boldsymbol{A})^{-1}\boldsymbol{W}^\top + \sigma_n^2\boldsymbol{I}. \tag{10}$$

Assigning the observed value of $\boldsymbol{y}$ to Eq. 9 and considering it as a function of the parameters, Eq. 9 is called a likelihood function, and its logarithm is a log-likelihood function. The value that maximizes the likelihood function, and hence the value that maximizes the log-likelihood function, is the ML estimate. Using the ML estimate of $\{\sigma_n^2, \sigma_h^2, \boldsymbol{a}\}$, $\boldsymbol{h}$ can be determined as the maximum a posteriori (MAP) estimator $\hat{\boldsymbol{h}}_{MAP}$, which maximizes the posteriori probability of $\boldsymbol{h}$ as follows:

$$\begin{aligned} p(\boldsymbol{h}|\boldsymbol{y}, \boldsymbol{a}, \sigma_n^2, \sigma_h^2) &= \frac{p(\boldsymbol{y}|\boldsymbol{h}, \sigma_n^2)p(\boldsymbol{h}|\boldsymbol{a}, \sigma_h^2)}{p(\boldsymbol{y}|\boldsymbol{a}, \sigma_n^2, \sigma_h^2)} \\ &\propto \exp\left[-\frac{1}{2}\left(\boldsymbol{h} - \hat{\boldsymbol{h}}_{MAP}\right)^\top \boldsymbol{V}_{h|y}^{-1}\left(\boldsymbol{h} - \hat{\boldsymbol{h}}_{MAP}\right)\right], \end{aligned} \tag{11}$$

$$\hat{\boldsymbol{h}}_{MAP} = \left(\frac{\boldsymbol{W}^\top\boldsymbol{W}}{\sigma_n^2} + \frac{\boldsymbol{A}^\top\boldsymbol{A}}{\sigma_h^2}\right)^{-1}\frac{\boldsymbol{W}^\top\boldsymbol{y}}{\sigma_n^2}, \tag{12}$$

$$\boldsymbol{V}_{h|y} = \left(\frac{\boldsymbol{W}^\top\boldsymbol{W}}{\sigma_n^2} + \frac{\boldsymbol{A}^\top\boldsymbol{A}}{\sigma_h^2}\right)^{-1}. \tag{13}$$

We can use $\hat{\boldsymbol{h}}_{MAP}$ as the recovery result of $\boldsymbol{h}$ by using the ML estimate $\{\hat{\sigma}_n^2, \hat{\sigma}_h^2, \hat{\boldsymbol{a}}\}$ as the values of the parameters in Eq. 12. Thus, the scheme of Bayesian estimation using the parameters estimated based on marginal likelihood is called empirical Bayesian method.

C. Algorithm Implementation by EM scheme

The MLE based on Eq. 9 generally requires iterative calculations, and each calculation is a little complicated. Instead, we can use an expectation-maximization (EM) algorithm where the MLE of the parameter and the MAP estimator of the latent variable are alternately updated by iterative calculation. In the EM algorithm, observation and latent variables are collectively referred to as complete data. The EM algorithm is effectively executed against the problem that the MLE of the parameter is easy when complete data is observed. Equation 8 corresponds

to the probability of complete data, and the log-likelihood function of complete data is formulated from Eq. 8 as follows:

$$\begin{aligned}&\ln L_c(\sigma_n^2, \sigma_h^2, \boldsymbol{a})\\ &= \mathrm{Const.} - \frac{N\ln\sigma_n^2}{2} - \frac{N\ln\sigma_h^2}{2} - \frac{\ln\det(\boldsymbol{A}^\top\boldsymbol{A})^{-1}}{2}\\ &\quad - \frac{(\boldsymbol{y}-\boldsymbol{W}\boldsymbol{h})^\top(\boldsymbol{y}-\boldsymbol{W}\boldsymbol{h})}{2\sigma_n^2} - \frac{\boldsymbol{h}^\top\boldsymbol{A}^\top\boldsymbol{A}\boldsymbol{h}}{2\sigma_h^2}. \end{aligned} \tag{14}$$

The following E-step and M-step are repeated until convergence.

In the E-step, we derive the expectation of Eq. 14 with respect to the posteriori probability of $\boldsymbol{h}$, $p(\boldsymbol{h}|\boldsymbol{y}, \hat{\sigma_n^2}^{(p)}, \hat{\sigma_h^2}^{(p)}, \hat{\boldsymbol{a}}^{(p)})$, where $\hat{\boldsymbol{\Theta}}^{(p)} \equiv (\hat{\sigma_n^2}^{(p)}, \hat{\sigma_h^2}^{(p)}, \hat{\boldsymbol{a}}^{(p)})$ is the estimate determined at the pth iteration. As a result, this expectation of Eq. 14, called the Q function, can be derived as follows:

$$\begin{aligned}&Q(\boldsymbol{\Theta}|\hat{\boldsymbol{\Theta}}^{(p)})\\ &= \mathrm{Const.} - \frac{N\ln\sigma_n^2}{2} - \frac{N\ln\sigma_h^2}{2} - \frac{\ln\det(\boldsymbol{A}^\top\boldsymbol{A})^{-1}}{2}\\ &\quad - \frac{\boldsymbol{y}^\top\boldsymbol{y} + 2\boldsymbol{y}^\top\boldsymbol{W}\hat{\boldsymbol{h}}^{(p)} + \mathrm{trace}\boldsymbol{W}\hat{\boldsymbol{V}}_h^{(p)}\boldsymbol{W}^\top}{2\sigma_n^2}\\ &\quad - \frac{\mathrm{trace}\boldsymbol{A}^\top\boldsymbol{A}\hat{\boldsymbol{V}}_h^{(p)}}{2\sigma_h^2}, \end{aligned} \tag{15}$$

$$\hat{\boldsymbol{h}}^{(p)} = \left(\frac{\boldsymbol{W}^\top\boldsymbol{W}}{\hat{\sigma_n^2}^{(p)}} + \frac{\hat{\boldsymbol{A}}^{(p)\top}\hat{\boldsymbol{A}}^{(p)}}{\hat{\sigma_h^2}^{(p)}}\right)^{-1}\frac{\boldsymbol{W}^\top\boldsymbol{y}}{\hat{\sigma_n^2}^{(p)}}, \tag{16}$$

$$\hat{\boldsymbol{V}}_h^{(p)} = \hat{\boldsymbol{h}}^{(p)}\hat{\boldsymbol{h}}^{(p)\top} + \left(\frac{\boldsymbol{W}^\top\boldsymbol{W}}{\hat{\sigma_n^2}^{(p)}} + \frac{\hat{\boldsymbol{A}}^{(p)\top}\hat{\boldsymbol{A}}^{(p)}}{\hat{\sigma_h^2}^{(p)}}\right)^{-1}. \tag{17}$$

In the M-step, $\hat{\boldsymbol{\Theta}}$ is updated so as to maximize the Q function derived as Eq. 15 with respect to $\boldsymbol{\Theta}$. For $\boldsymbol{a}$, we need to maximize the 4th and 6th terms on the right hand side of Eq. 15. When the number of observation is sufficiently large, since the 6th term is $O(N)$, the 4th term can be neglected as compared to the 6th term. Therefore, in this study, we update $\hat{\boldsymbol{a}}$ to satisfy the following equation.

$$\mathrm{trace}\frac{\partial(\boldsymbol{A}^\top\boldsymbol{A})}{\partial\boldsymbol{a}}\hat{\boldsymbol{V}}_h^{(p)} = \boldsymbol{0}. \tag{18}$$

Both variances are updated as follows:

$$\hat{\sigma_n^2}^{(p+1)} = \frac{\boldsymbol{y}^\top\boldsymbol{y} + 2\boldsymbol{y}^\top\boldsymbol{W}\hat{\boldsymbol{h}}^{(p)} + \mathrm{trace}\boldsymbol{W}\hat{\boldsymbol{V}}_h^{(p)}\boldsymbol{W}^\top}{N}, \tag{19}$$

$$\hat{\sigma_h^2}^{(p+1)} = \frac{\mathrm{trace}\hat{\boldsymbol{A}}^{(p+1)\top}\hat{\boldsymbol{A}}^{(p+1)}\hat{\boldsymbol{V}}_h^{(p)}}{N}. \tag{20}$$

The above two steps are repeated and update is stopped when the change of $\hat{\boldsymbol{\Theta}}$ becomes sufficiently small. $\hat{\boldsymbol{\Theta}}^{(p)}$ obtained when converging corresponds to the MLE, and also $\hat{\boldsymbol{h}}^{(p)}$ is the MAP estimator.

III. Numerical Evaluation

A. Evaluation Method

Numerical performance evaluation of our method was done using ideal data satisfying Eq. 1. As the number of cycles included in the transmission pulse increases, the observed frequency band decreases, and it becomes difficult to estimate the AR parameters and hence, to recover $\boldsymbol{h}$. Impulse, 1 cycle of 5 MHz and 5 cycles of 5 MHz were used as the transmission pulse. Of the above, two 5 MHz pulses were apodized by Gaussian window function. Observing the echo generated by impulse transmission, it is expected that $\boldsymbol{h}$ can be almost completely restored. This is because the entire frequency band can be observed. Observation data $\boldsymbol{y}$ was prepared by the following procedure.

1) We set $\boldsymbol{a}$ and σ_h^2, and use these to generate $\boldsymbol{h}$ as AR time series.
2) $\boldsymbol{h}$ is convoluted with the transmission pulse selected from the above three, and the result corresponds to $\boldsymbol{y}$ with no noise.
3) We set σ_n^2 and use it to generate Gaussian noise. This noise is added to $\boldsymbol{y}$ generated above to obtain observation data.

Transducer characteristics, beam focusing and propagation attenuation were ignored and data exactly matched to the evaluation model were used for evaluation.

Performance evaluation that depends on the order of AR model and AR coefficient will be a subject for the future, and we set the order to 2 and fixed the parameters $\boldsymbol{a} = \{0.6, 0.3\}$ and $\sigma_h^2 = 0.02$. In that case, each value of generated $\boldsymbol{h}$ remained almost in the range of ± 1. We also set the noise variance $\sigma_n^2 = 0.02$, and the peak amplitude of the transmission pulse was normalized to 1.0. Under this condition, the standard deviation of noise was 2.5% of the standard deviation of $\boldsymbol{y}$ when transmitting a pulse consisting of one cycle, and 1.2% when transmitting a pulse consisting of 5 cycles. Since it is assumeobservation noise is electric noise, we can suppose that σ_n^2 is known in advance with no practical problem.

B. Results

In this study, 10 time series of echo consisting of 1000 sampling values were used. The time sampling rate is about 100 points per 5 MHz sinusoidal cycle common to all processing. For all trials performed, we confirmed that the EM algorithm had almost converged by 500 iterative updates, therefore we adopt $\hat{\boldsymbol{h}}^{(500)}$ as an estimation result and simply write it as $\hat{\boldsymbol{h}}$. An example of the setting value of $\boldsymbol{h}$ to be recovered is shown in Fig. 1. Instead of ensemble average, the power spectrum in Fig. 1(b) was calculated by taking the average value of 10 series of $\boldsymbol{h}$. The power spectrum density (PSD) $P(f)$ of the AR model can theoretically be formulated as follows:

$$P(f) = \frac{\sigma_h^2}{|1 - \sum_{i=1}^{P} a_i e^{-j2\pi f}|^2}, \tag{21}$$

and the theoretical value corresponding to the assumed AR model is shown in Fig. 1(b) as a red curve.

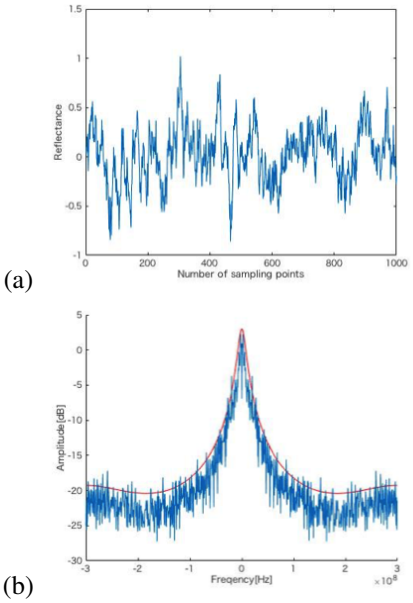

Fig. 1. One series of $\boldsymbol{h}$ consisting of 1,000 samples is shown in (a), and its power spectrum is shown in (b). The red curve in (b) indicates the theoretical power spectrum of the set AR model.

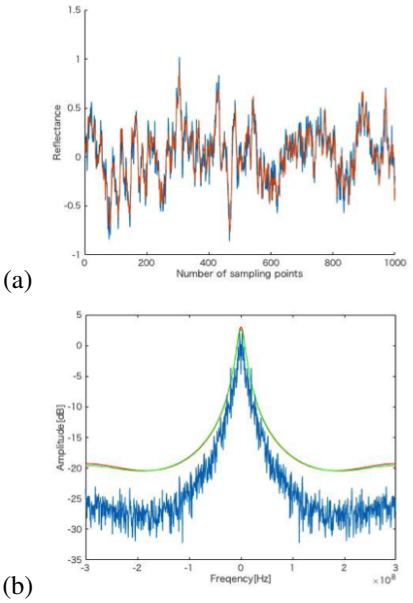

Fig. 3. $\hat{\boldsymbol{h}}$ restored for impulse transmission is indicated by red line in (a) and blue line is set value. The PSD is shown in (b), the red curve corresponds to the theoretical value of the set AR model, and the green curve corresponds to the theoretical value of the estimated AR model.

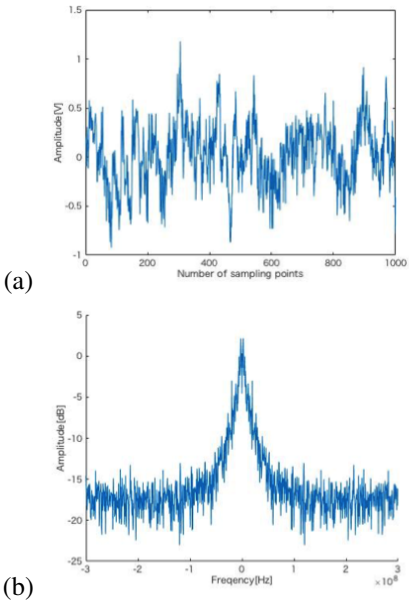

Fig. 2. The echo $\boldsymbol{y}$ generated by convolving the impulse with $\boldsymbol{h}$ and adding observation noise is shown in (a) and its PSD is shown in (b).

Firstly, we attempted to restore $\hat{\boldsymbol{h}}$ when the transmission pulse is impulse. In this case, almost all frequencies are observed, and only observation noise hinders estimation. Figure 2 shows the echo signal $\boldsymbol{y}$ and its power spectrum. Since the observation noise exists, the level of high frequency components in Fig. 2(b) rise compared to the power spectrum of $\boldsymbol{h}$ in Fig. 1(b). The $\hat{\boldsymbol{h}}$ corresponding to Fig. 1(a) is indicated by a red line in Fig. 3(a), and its power spectrum is also shown in Fig. 3(b), in which the red curve and the green curve show respectively the theoretical values of the set AR model and the theoretical values of the estimated AR model, both of which are approximately equal. Estimated AR parameters are $\hat{\boldsymbol{a}} = \{0.618, 0.278\}$ and $\hat{\sigma_h^2} = 0.0198$. From this result, it can be seen that the AR model can be estimated with extremely high accuracy. Regarding the recovery of $\boldsymbol{h}$, it is difficult to obtain the white noise component in principle, and in the high frequency band in Fig. 3(b), the restoration error appears conspicuously.

Next, we estimated the AR parameters and restore $\boldsymbol{h}$ from the echo generated by one cycle pulse transmission. As in Fig. 2, $\boldsymbol{y}$ and its PSD are shown in Fig. 4. Comparing Fig. 2 and Fig. 4, it can be seen that one cycle pulse transmission restricts the observable frequency band to a low range. The restored $\hat{\boldsymbol{h}}$ is shown in Fig. 5, and the estimated parameters are $\hat{\boldsymbol{a}} = \{0.589, 0.313\}$ and $\hat{\sigma_h^2} = 0.0185$, and the estimation error is slightly larger than in the case of impulse transmission. Although it can be easily predicted that the restoration problem from very limited observation is a difficult task, AR model can be estimated with high accuracy. The reason for this is presumed to be that the local frequency component has sufficient information to restore the AR model as extrapolation. This characteristic seems to be weakened as the order of the AR model increases, that is, as the degree of freedom of the AR model increases. In Fig. 5(b), there is little difference between the red curve showing the theoretical PSD of the true model and the green curve of the estimated model. Comparing Fig. 5(b) with Fig. 4(b), it is clear that the PSD of $\hat{\boldsymbol{h}}$ becomes obviously a wide band and approaches the PSD of the set value in Fig. 1. In other words, a part not in the high frequency band of the unobservable frequencies can be effectively restored by assuming the AR model.

Finally, $\boldsymbol{y}$ and $\hat{\boldsymbol{h}}$ for 5 cycles pulse transmission are

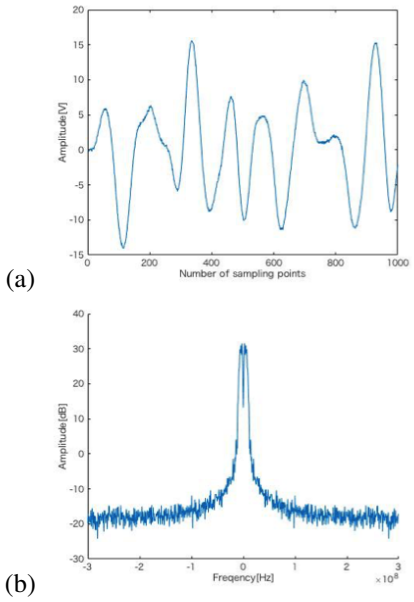

Fig. 4. The echo $\boldsymbol{y}$ generated by convolving the one cycle pulse with $\boldsymbol{h}$ and adding observation noise is shown in (a) and its PSD is shown in (b).

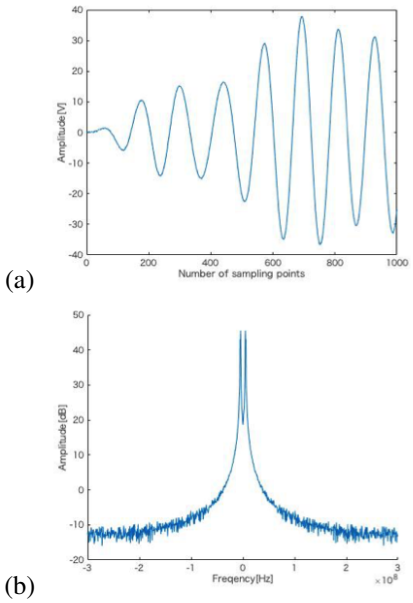

Fig. 6. The echo $\boldsymbol{y}$ generated by convolving the 5 cycles pulse with $\boldsymbol{h}$ and adding observation noise is shown in (a) and its PSD is shown in (b).

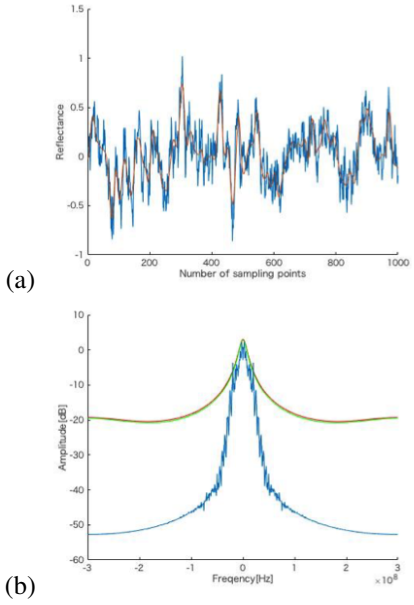

Fig. 5. $\hat{\boldsymbol{h}}$ restored for one cycle pulse transmission is indicated by red line in (a) and blue line is set value. The PSD is shown in (b), the red curve corresponds to the theoretical value of the set AR model, and the green curve corresponds to the theoretical value of the estimated AR model.

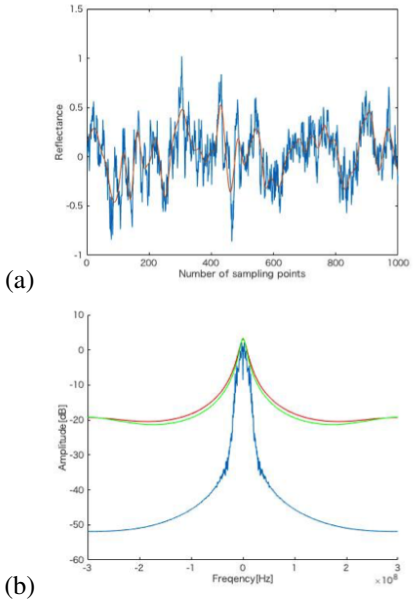

Fig. 7. $\hat{\boldsymbol{h}}$ restored for 5 cycles pulse transmission is indicated by red line in (a) and blue line is set value. The PSD is shown in (b), the red curve corresponds to the theoretical value of the set AR model, and the green curve corresponds to the theoretical value of the estimated AR model.

shown in Figs. 6 and 7. The parameters are estimated as $\hat{\boldsymbol{a}} = \{0.546, 0.365\}$ and $\hat{\sigma_h^2} = 0.0168$. Since the frequency band to be observed is further limited, the estimation error of the parameters is slightly larger than the estimation error of the one cycle transmission. However, the theoretical PSD computed using $\hat{\boldsymbol{a}}$ and $\hat{\sigma_h^2}$ is sufficiently close to that of the true model.

The above result are better than expected and it was confirmed that the empirical Bayesian method is very useful for latent variable estimation where the observation is limited and the parameters of the prior knowledge of the latent variable are unknown. Such a problem is often to be solved[18]. For comparison, the estimates simply restored by Eq. 2 are shown in Fig. 8, where the singular values of $\boldsymbol{W}$ greater than σ_n^2 are used to define $\boldsymbol{W}^+$. As a result of observation noise amplification, $\hat{\boldsymbol{h}}$ shown by a red line has large noisy component. These results relatively indicate the effectiveness of the application of empirical Bayesian estimation.

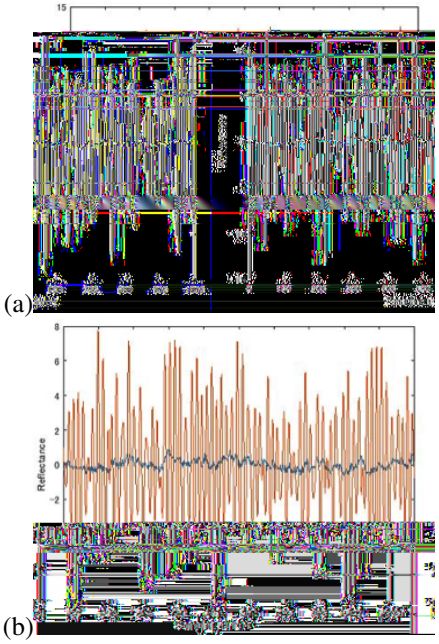

Fig. 8. $\hat{\boldsymbol{h}}$ obtained by pseudo-inverse filtering for 1 cycle pulse transmission is shown in (a) and that for 5 cycle pulse transmission is shown in (b). Red line indicates $\hat{\boldsymbol{h}}$ and blue line indicates set $\boldsymbol{h}$.

IV. Conclusions

In this study, in order to restore scatterer distribution from ultrasonic echo, empirical Bayesian method was applied. Although AR model identification is usually performed directly on the observed time series, in this problem, it is a latent time series that model identification should be done, and the identification is impossible with the well-known Levinson-Durbin algorithm. In identifying and restoring the latent time series in this study, ill-posed characteristic is strong, that is, observations are largely restricted. However, we confirmed through ideal data simulations that the empirical Bayes could properly solve the problem.

The simulations was carried out only under restricted conditions, and there are some important matters to be confirmed. Firstly, the performance of the empirical Bayes against the higher order AR models should be evaluated. Various complicated conditions, for example, the characteristics of a transducer and of a propagation medium should be considered. To do so, we are advancing simulations based on finite element method (FEM) using PZFlex, a standard FEM code for ultrasound analysis. Since the echo generation process is complicated and depends not only reflection but also transmittance and diffraction, it is difficult in principle to restore the reflectance of the scatterers purely. However, the obtained $\hat{\boldsymbol{h}}$ contains information on the tissue, and we expect to be able to diagnose tissue properties from the change $\hat{\boldsymbol{h}}$.

In the next stage, we are going to examine a new imaging system that presents organ boundaries and inside the organ separately. By subtracting the echo corresponding to the image of the inside the organ, that is obtained by the method in this study, from the original echoes, and subsequently applying a method to extract the organ boundaries, the imaging system above is expected to be constructed.

Acknowledgment

The part of this work was supported by the research fund of Konica Minolta, Inc., Japan.

References

[1] Q. Liang, I. Wendelhag, J. Wikstrand, T. Gustavsson, "A multiscale dynamic programming procedure for boundary detection in ultrasonic artery images," IEEE Trans. Medical Imaging, vol. 19, no. 2, pp. 127–142, 2000.

[2] J. A. Noble and D. Boukerroui, "Ultrasound image segmentation: a survey," IEEE Trans. Medical Imaging, vol. 25, no. 8, pp. 987–1010, 2006.

[3] M. E. Plissiti, D. I. Fotiadis, L. K. Michalis, G. E. Bozios, "An automated method for lumen and media-adventitia border detection in a sequence of IVUS frames," IEEE Trans. Information Tech. in Biomedicine, vol. 8, no. 2, pp. 131–141, 2004.

[4] K. Z. Abd-Elmoniem, A.-B. M. Youssef, Y. M. Kadah, "Real-time speckle reduction and coherence enhancement in ultrasound imaging via nonlinear anisotropic diffusion," IEEE Trans. Biomedical Eng., vol. 49, no. 9, pp. 997-1014, 2002.

[5] F. Zhang, Y. Mo Yoo, L. Mong Koh, Y. Kim, "Nonlinear diffusion in Laplacian pyramid domain for ultrasonic speckle reduction," IEEE Trans. Medical Imaging, vol. 26, no. 2, pp. 200-211, 2007.

[6] J. R. Sanchez, M. L. Oeize, " An ultrasonic imaging speckle-suppression and contrast-enhancement technique by means of frequency compounding and coded excitation," IEEE Trans. UFFC, vol. 56, no. 7, pp. 1327–1339, 2009.

[7] S. K. Narayanan and R. S. D. Wahidabanu, "A view on despeckling in ultrasound imaging," Int. Journal. Signal Processing, Image Processing and Pattern Recognition, vo. 2, no. 3, pp. 85–98, 2009.

[8] D. Friboulet, H. Liebgott, R. Prost, "Compressive sensing for raw RF signals reconstruction in ultrasound," Proc. IEEE IUS, pp. 367–370, 2010.

[9] H. Liebgott, R. Prost, D. Friboulet, "Pre-beamformed RFsignal reconstrcution in medical ultrasound using compressive sensing," Ultrasonics, vol. 53, no. 2, pp. 525–533, 2013.

[10] N. Wagner, Y. C. Eldar, Z. Friedman, "Compressed beamforming in ultrasound imaging," Proc. IEEE Trans. Signal Processing, vol. 60, no. 9, pp. 4643–4657, 2012.

[11] A. Achim, B. Buxton, G. Tzagkarakis, P. Tsakalides, "Compressive sensing for ultrasound RF echoes using a-stable distributions," Proc. IEEE Annual Int. Conf. Eng. Medicine and Biology Society, pp. 4304–4307, 2010.

[12] H. Suzuki, N. Tagawa, K. Okubo, "A study on speckle reduction based on stochastic fluctuation of transmitted ultrasound beam," Proc. IEEE IUS, pp. 910–913, 2013.

[13] T. Wada, Y. Ho, K. Okubo, N. Tagawa, Y. Hirose "High frame rate super resolution imaging based on ultrasound synthetic aperture scheme," Physics Procedia, vol. 70, pp. 1216-1220, 2015.

[14] T. Yamamura, M. Tanabe, K. Okubo, N. Tagawa, "A method for improving signal-to-noise ratio of tissue harmonic imaging based on Bayesian inference using information of fundamental echoes," Jpn. J. Appl. Phys., vol. 51, 07GF01(12 pages), 2012.

[15] T. Hiraoka, N. Tagawa, K. Okubo, Y. Ho, I. Akiyama, "Compensation method for frequency dependent attenuation for tissue harmonic imaging," Proc. IEEE IUS, pp. 1085–1088, 2014.

[16] B. P. Carlin, T. A. Louis, " Bayes and empirical Bays methods for data analysis," Statistics and Computing, vol. 7, no. 2, pp. 153–154, 1997.

[17] D. P. Wipf and B. D. Rao, "An empirical Bayesian strategy for solving the simultaneous sparse approximation problem," IEEE Trans. Signal Processing, vol. 55, no. 7, pp. 3704–3716, 2007.

[18] N. Tagawa, S. Tsukada, "Selective use of appropriate image pairs for shape from multiple motions based on gradient method," Proc. Int. Conf. Computer vision Theory and Applications, pp. 554-563, 2016.